

# **Parametric net influx rate images of $^{68}\text{Ga}$ -DOTATOC and $^{68}\text{Ga}$ -DOTATATE: quantitative accuracy and improved image contrast**

Ezgi Ilan<sup>1,2</sup>, Mattias Sandström<sup>1,2</sup>, Irina Velikyan<sup>1,3</sup>, Anders Sundin<sup>1,3</sup>, Barbro Eriksson<sup>4</sup>, Mark Lubberink<sup>1,2</sup>

<sup>1</sup>Section of Nuclear Medicine and PET, Department of Surgical Sciences, Uppsala University, Uppsala, Sweden; <sup>2</sup>Medical Physics, Uppsala University Hospital, Uppsala, Sweden; <sup>3</sup>PET-centre, Medical Imaging Centre, Uppsala University Hospital, Uppsala, Sweden. <sup>4</sup>Department of Medical Science, Section of Endocrine Oncology, Uppsala University Hospital, Uppsala, Sweden.

## **Correspondence and reprints requests:**

Ezgi Ilan, Uppsala University Hospital, Medical Physics, SE-751 85 Uppsala, Sweden,  
Telephone number: +46 18 611 27 51, E-mail: [ezgi.ilan@akademiska.se](mailto:ezgi.ilan@akademiska.se)

**Word count:** 4907 words

**Running foot line:** Validation of net influx rate images

## **ABSTRACT**

$^{68}\text{Ga}$ -DOTATOC and  $^{68}\text{Ga}$ -DOTATATE are radiolabelled somatostatin analogs used for diagnosis of somatostatin receptor expressing neuroendocrine tumors (NETs) and standardized uptake value (SUV) –measurements are suggested for treatment monitoring. However, changes in net-influx rate ( $K_i$ ) may better reflect treatment effects than those of the SUV, and accordingly there is a need to compute parametric images showing  $K_i$  at the voxel level. The aim of this study was to evaluate parametric methods for computation of parametric  $K_i$  images by comparison to volume of interest based methods and to assess image contrast in terms of tumor-to-liver ratio.

### **Methods**

Ten patients with metastatic NETs underwent a 45-min dynamic positron emission tomography (PET) examination followed by whole-body PET/CT at 1 h post injection of  $^{68}\text{Ga}$ -DOTATOC and  $^{68}\text{Ga}$ -DOTATATE on consecutive days. Parametric  $K_i$  images were computed using a basis function method (BFM) implementation of the two tissue irreversible compartment model and the Patlak method using a descending aorta image-derived input function, and mean tumor  $K_i$  values were determined for 50% isocontour volume of interest (VOIs) and compared to  $K_i$  values based on non-linear regression (NLR) of the whole-VOI time-activity curve. A subsample of healthy liver was delineated in the whole-body and  $K_i$  images and tumor-to-liver ratios were calculated in order to evaluate image contrast. Correlation and agreement between VOI-based and parametric  $K_i$  values were assessed using regression and Bland-Altman analysis.

## Results

Correlation ( $R^2$ ) between NLR-based and parametric image-based (BFM) tumor  $K_i$  values was 0.98 (slope 0.81) and 0.97 (slope 0.88) for  $^{68}\text{Ga}$ -DOTATOC and  $^{68}\text{Ga}$  DOTATATE, respectively. For Patlak analysis, correlation between NLR-based and parametric based (Patlak) tumor  $K_i$  were 0.95 (slope 0.71) and 0.92 (slope 0.74) for  $^{68}\text{Ga}$ -DOTATOC and  $^{68}\text{Ga}$ -DOTATATE, respectively. There was no bias between NLR and parametric based  $K_i$ -values. Tumor-to-liver contrast was 1.6 and 2.0 times higher in the parametric BFM- $K_i$  images, and 2.3 and 3.0 times in the Patlak images, than in the whole-body images for  $^{68}\text{Ga}$ -DOTATOC and  $^{68}\text{Ga}$ -DOTATATE, respectively.

## Conclusion

A high correlation and agreement between NLR- and parametric based  $K_i$  values was found, showing that  $K_i$  images are quantitatively accurate. In addition, tumor-to-liver contrast was superior in the parametric  $K_i$  images compared to whole-body images both for  $^{68}\text{Ga}$ -DOTATOC and  $^{68}\text{Ga}$  DOTATATE.

**Key words:**  $^{68}\text{Ga}$ -DOTATOC;  $^{68}\text{Ga}$ -DOTATATE; Parametric images; Net influx rate;

Neuroendocrine tumors

## INTRODUCTION

Neuroendocrine tumors (NETs) are tumors derived from the disseminated system of endocrine cells in the body and have diverse biological and clinical characteristics (1). Epidemiological studies have shown that the NET incidence is rising and according to an analysis of the North American Surveillance, Epidemiology, and End Results registry data the annual age-adjusted incidence increased from 1.09/100,000 in 1973 to 5.25/100,000 in 2004. The reason for this is assumed to be the improvements in imaging technology (2).

NETs are characterized by cellular overexpression of somatostatin receptors (SSTR) allowing for the use of unlabeled and radiolabeled somatostatin analogs (SSA) for imaging and therapy. SSTR scintigraphy with the indium-111-labeled SSA, <sup>111</sup>In-DTPA-octreotide (OctreoScan®) remains the mainstay for functional NET imaging and continues to play an important role for NET imaging (3, 4). However, positron emission tomography (PET) using Gallium-68 (<sup>68</sup>Ga)-labeled SSAs, such as <sup>68</sup>Ga-DOTATOC, <sup>68</sup>Ga-DOTANOC and <sup>68</sup>Ga-DOTATATE, is gradually replacing SSTR scintigraphy and is expected to become the future gold standard for SSTR imaging of NETs (5). Positron emission tomography/computed tomography (PET/CT) with <sup>68</sup>Ga-SSA shows a specificity and sensitivity well above 90 %, exceeding that of Octreoscan® and computed tomography (CT) (6-11).

In disseminated disease, unlabeled SSA constitutes first line therapy for low grade NETs. During the last decade, peptide receptor radionuclide therapy (PRRT), with radiolabeled SSAs such as <sup>177</sup>Lu-DOTA-D-Phe<sup>1</sup>-Tyr<sup>3</sup>-octreotate (<sup>177</sup>Lu-DOTATATE) and <sup>90</sup>Y-DOTA-D-Phe<sup>1</sup>-Tyr<sup>3</sup>-octreotide (<sup>90</sup>Y-DOTATOC) has shown to be effective and plays an increasingly important role in

the treatment of NET patients (12-21). However, large interpatient variability in organ distribution and consequently radiation dose delivered to the lesions and normal organs calls for development of methods for individualized radiotherapy planning (22). Conventional radiological imaging techniques such as CT and magnetic resonance imaging are well established for evaluation of therapy response in the clinical routine by assessing changes in tumor size and diagnosing new lesions. The Response Evaluation Criteria in Solid Tumors (23), are, however, not optimal to monitor systemic NET therapies because tumor shrinkage is seen only in a small fraction of patients and instead the treatments mainly induce tumor stabilization. Moreover, PRRT induces long-time effects due to  $\beta^-$ -emission of  $^{177}\text{Lu}$  and  $^{90}\text{Y}$  resulting in continuously increasing necrosis and decrease of viable tumor although the tumor size may appear unchanged during the subsequent examinations (24). Also, with the new so-called targeted therapies tumor shrinkage is less common and heterogeneous nature of tumors also adds uncertainty to such measurements. There is therefore a need for new methods to evaluate NET therapy response besides conventional morphological size criteria (25).

In parallel with the increasing use of  $^{18}\text{F}$ -FDG-PET/CT for therapy monitoring in conventional oncology, this application has also been suggested for NETs. However, because of the low proliferation and low metabolic activity of NET cells, they are generally not  $^{18}\text{F}$ -FDG avid (26). By contrast, the large majority of NETs expresses SSTRs and shows high  $^{68}\text{Ga}$ -SSA uptake. Consequently,  $^{68}\text{Ga}$ -DOTATOC and  $^{68}\text{Ga}$ -DOTATATE have been tested to assess NET therapy response (6, 24, 27). In one study (24) the authors found that the changes in tumor standardize uptake value (SUV) between baseline and follow-up  $^{68}\text{Ga}$ -DOTATOC-PET/CT did not correlate to the outcome of PRRT. This was also found in another study (27), although changes in the tumor-to-spleen SUV ratio between baseline and follow-up  $^{68}\text{Ga}$ -DOTATOC were shown more

accurate than changes in tumor  $SUV_{max}$  to evaluate the response to PRRT. The problems of applying static tumor uptake measurements in these two therapy monitoring studies may be explained, at least partly, by the results in a recent study (6) on  $^{68}Ga$ -DOTATOC and  $^{68}Ga$ -DOTATATE. In this study, SUV saturated at a static value for high net uptake rate  $K_i$ , especially for higher SUV values (>20-25). Hence, SUV does not appear to reflect SSTR density for tumors with high receptor expression. Consequently, changes in  $K_i$  may better reflect treatment response than changes in SUV.

In order to facilitate the clinical use of  $K_i$ , accurate and reliable computation of parametric images showing  $K_i$  at the voxel level is desirable. Moreover, information on  $K_i$  at voxel level provides information on tumor heterogeneity that is lost when average tumor  $K_i$  is assessed. The aim of this study was to evaluate methods for computation of parametric  $K_i$  images by comparison to volume of interest (VOI)-based methods. A secondary aim was to explore the conditions for lesion detection in  $K_i$  images by assessing the image contrast in terms of tumor-to-liver ratios compared to those in static SUV images.

## **MATERIALS AND METHODS**

### **Patients**

Ten patients (6 men and 4 women; mean age  $\pm$  SD,  $65 \pm 10$  y) diagnosed with disseminated gastroenteropancreatic NETs, confirmed by histopathology, were included in the study. Five patients had small-intestinal NETs, three had pancreatic NETs and two had lung carcinoids. The total number of tumors included in the study was 16; five patients had one tumor, one had two

tumors and three had three tumors. Only tumors with diameter > 1 cm and high uptake (determined visually) were included. The study was approved by the Regional Ethical Review Board in Uppsala and the Radiation Ethics Committee at Uppsala University Hospital, and the patients all signed a written informed consent prior to inclusion in the study.

### **Image acquisition and Reconstruction**

Each patient underwent a  $^{68}\text{Ga}$ -DOTATOC and a  $^{68}\text{Ga}$ -DOTATATE-PET/CT examination on consecutive days, in random order. The patients received a bolus injection of  $86.9 \pm 16.4$  MBq (range, 61-113 MBq)  $^{68}\text{Ga}$ -DOTATOC and  $91.4 \pm 18.7$  MBq (range, 67-121 MBq) of  $^{68}\text{Ga}$ -DOTATATE. Good manufacturing practice-compliant production of  $^{68}\text{Ga}$ -DOTATOC and  $^{68}\text{Ga}$ -DOTATATE was accomplished as previously described (6, 28).

Images were acquired on a Discovery ST PET/CT scanner (GE-Healthcare) with a transaxial- and axial field of view of 70 and 15.7 cm, respectively. The image matrix size was 128 x 128 with a voxel size of 3.9 x 3.9 x 3.27 mm. The patients underwent a low-dose CT scan (140 kV, auto mA 20-80 mA) followed by a 45-min dynamic PET examination of the abdomen to include the major tumor load. The dynamic PET examination started simultaneously with the intravenous injection of  $^{68}\text{Ga}$ -DOTATOC or  $^{68}\text{Ga}$ -DOTATATE and consisted of 22 time frames of increasing durations (6 x 10, 3 x 20, 3 x 60, 5 x 180, 5 x 300 s). The dynamic examination was followed by a whole-body PET/CT scan ranging from the proximal femur to the base of the skull (3 min per bed position) starting at 60 min p.i. following a second low-dose CT for attenuation correction of the whole-body images. Peripheral venous blood samples (circa 1 ml) were taken at 5, 20, 45, and 60 min p.i. to assess the whole-blood and plasma radioactivity concentrations, respectively. The PET data were normalized and corrected for dead time, random coincidences, scatter and attenuation

and were reconstructed using ordered subsets expectation maximization (OSEM) with 2 iterations and 21 subsets applying a 5.4 mm Gaussian post-filter.

### **Image-derived input functions**

Since labeling with  $^{68}\text{Ga}$ -DOTATOC/DOTATATE is stable during the duration of the PET-examination, the total radioactivity concentration in the arterial plasma was used as input function (6). Circular regions of interest with a diameter of 1 cm were drawn over the descending aorta in 10 consecutive images planes in the time frame in which the first passage of the bolus was best visualized (typically frame 1-10). These regions of interest were then combined to form a single aortic VOI. The resulting aortic VOI was projected onto all time frames in the dynamic examination to produce an arterial time-activity curve. The image-derived input functions were calculated by multiplying the arterial time-activity curve with the mean plasma to whole blood ratio in venous blood (29, 30).

### **VOI-based kinetic analysis**

Fifty percent isocontour tumor VOIs were drawn in the 20-45 min summation image of the dynamic data and were projected onto all time frames to generate tumor time-activity curves, using the NEDPAS software developed at VU University Medical Centre (Amsterdam) (31). The tumors were delineated similarly in the whole-body images and the corresponding tumor SUVs were derived. In order to evaluate the tumor-to-liver contrast, a subsample of healthy liver was delineated in the whole-body images using a spherical 20-ml VOI.



It has previously been shown that the kinetics of  $^{68}\text{Ga}$ -DOTATOC/DOTATE can be described by an irreversible two-tissue compartment model (32-36), which reflects internalization of the receptor-ligand complex. From this compartment model the following differential equations can be defined:

$$\frac{dC_1(t)}{dt} = K_1 C_P(t) - (k_2 + k_3) C_1(t) \quad (1)$$

where  $C_1(t)$  is the concentration of free tracer in tissue,  $C_P(t)$  is the concentration in plasma,  $K_1$ ,  $k_2$  and  $k_3$  are rate constants, and:

$$\frac{dC_2(t)}{dt} = k_3 C_1(t) \quad (2)$$

where  $C_2(t)$  is the concentration of tracer internalized into the tumor cell. The solution of this model, with the addition of a blood volume component, is given by following equation:

$$C_{PET}(t) = (K_1 - K_i) e^{-(k_2+k_3)t} \otimes C_P(t) + K_i \otimes C_P(t) + V_A C_A(t) \quad (3)$$

in which  $C_{PET}(t)$  represents the measured concentration,  $V_A$  represents arterial blood volume,  $C_A(t)$  the arterial blood concentration and  $K_i$  the net uptake rate (37) defined as:

$$K_i = \frac{K_1 k_3}{k_2 + k_3} \quad (4)$$

By fitting equation 3 to the measured PET data using non-linear regression (NLR),  $K_i$  can be determined, which is assumed to reflect a combination of receptor density and the ability of the ligand to internalization in the tumors (6).

### **Parametric image analysis**

Parametric  $K_i$  images were generated firstly by a basis function method (BFM) implementation of the irreversible two-tissue compartment model (38, 39), and secondly by applying the Patlak method (37, 40) ( $t^* = 15$  min p.i) on the dynamic PET data 15-45 min post injection, using in-house-developed software in MATLAB. For the BFM implementation, 20 logarithmically spaced exponential clearance rates ( $\alpha=k_2+k_3$ ) ranging between 0.1 and 0.8  $\text{min}^{-1}$  were used in addition to an irreversible basis function to create a set of basis functions:

$$BF_i = e^{-\alpha_i t} \otimes C_P(t) \quad (4)$$

The linear combination of the three terms in equation 3, using  $BF_i$  that resulted in the minimum sum of squared residuals, yielded  $K_1-K_i$ ,  $K_i$ , and  $V_A$  for each voxel. Prior to parametric computations, a Gaussian filter with full width at half maximum (FWHM) of 5 mm was applied. Mean tumor  $K_i$  values were determined for 50% iso-contour VOIs in the parametric images. Liver VOIs were drawn in the parametric  $K_i$  images (as described above for the whole-body images), and tumor-to-liver ratios were calculated.

## **Statistical analysis**

The agreement and correlation between the VOI-based and parametric-based  $K_i$  values were determined using, Pearson correlation, Deming regression and Bland-Altman analysis (GraphPad Software, Inc, Prism Version 6.04, San Diego, California).

## **RESULTS**

### **VOI and parametric based kinetic analysis**

A linear relation was found between the VOI-based and parametric-based  $K_i$  values both for  $^{68}\text{Ga}$ -DOTATOC and  $^{68}\text{Ga}$ -DOTATATE. The relations between the VOI-based (NLR) and parametric-based (BFM and Patlak)  $K_i$  values for  $^{68}\text{Ga}$ -DOTATOC and  $^{68}\text{Ga}$ -DOTATATE are shown in Figure 1. Pearson correlation coefficients, Deming regression slope and bias for the VOI (NLR) and parametric based (BFM and Patlak)  $K_i$  are listed in Table 1. For both tracers, the Pearson correlation coefficient was higher for BFM than for Patlak, the slope of regression line was higher for BFM than for Patlak (Table 1) and no significant bias was found for either parametric method or tracer.

Parametric  $K_i$  values determined by BFM and Patlak for  $^{68}\text{Ga}$ -DOTATOC and  $^{68}\text{Ga}$ -DOTATATE are illustrated in Figures 2A and 2B, respectively. The Pearson correlation coefficient between BFM and Patlak  $K_i$ -values was 0.99 for  $^{68}\text{Ga}$ -DOTATOC and 0.98 for  $^{68}\text{Ga}$ -DOTATATE. The Deming regression line slope between BFM and Patlak  $K_i$ -values was 0.88 for  $^{68}\text{Ga}$ -DOTATOC and 0.85 for  $^{68}\text{Ga}$ -DOTATATE. The bias from the Bland-Altman plots were 0.01 (95%

confidence interval= -0.05 to 0.03) and 0.01 (95% confidence interval= -0.08 to 0.06) for  $^{68}\text{Ga}$ -DOTATOC and  $^{68}\text{Ga}$ -DOTATATE, respectively.

### **Tumor-to-liver contrast**

The image contrast visually improved in the parametric  $K_i$  images both for  $^{68}\text{Ga}$ -DOTATOC and  $^{68}\text{Ga}$ -DOTATATE (Fig. 3) and the tumor-to-liver ratio was generally higher in the parametric  $K_i$  images than in the whole-body images (Fig. 4). The tumor-to-liver ratio was 1.6 and 2.0 times higher in the parametric  $K_i$  images based on BFM than in the whole-body images for  $^{68}\text{Ga}$ -DOTATOC and  $^{68}\text{Ga}$ -DOTATATE (Fig. 4A), respectively. For the parametric  $K_i$  images based on Patlak method the tumor-to-liver ratio was 2.3 and 3.0 times higher than in the whole-body images for  $^{68}\text{Ga}$ -DOTATOC and  $^{68}\text{Ga}$ -DOTATATE (Fig. 4B), respectively. Generally, the image contrast was higher for  $^{68}\text{Ga}$ -DOTATATE than for  $^{68}\text{Ga}$ -DOTATOC (Fig. 4).

## **DISCUSSION**

Early prediction of treatment response is essential to guide tumor therapy and avoid unnecessary side effects and costs from ineffective treatments. SUV has been proposed as a marker of SSTR density but changes of tumor SUV at  $^{68}\text{Ga}$ -DOTATOC-PET/CT during PRRT have not been found to reliably correlate with the patient outcome (24, 27, 41-43). It was previously shown that  $K_i$  and SUV are not linearly correlated for NETs (especially for higher SUV values >20-25), and the former may more adequately reflect the tumor SSTR density than SUV (6). However, in the present study,  $k_3$  was found to be much higher than  $k_2$  in patients with high  $K_i$ , which indicates flow-limited delivery and an associated underestimation of both  $K_i$  and SUV, so this cannot

explain the previously observed divergence between  $K_i$  and SUV. A more detailed analysis showed that the difference between SUV and  $K_i$  can rather be attributed to faster plasma clearance in patients with a high receptor burden, since the plasma radioactivity concentration at 45 min p.i. in patients with high  $K_i$  values was considerably lower than in patients with low  $K_i$  values. This, in turn, would not affect the accuracy of  $K_i$  since plasma concentrations are taken into account when estimating  $K_i$ , but it does affect SUV since the absolute amount of tracer taken up into tissue is limited by the low plasma activity concentrations. Possibly, the total amount of receptors in these patients is so high that nearly all peptide is cleared from the plasma during the scan, leading to the apparent saturation of SUV values.

The primary aim of this study was to develop a method to compute images that would incorporate the  $K_i$  parameter allowing more accurate determination of receptor density as well as to compare NLR- and parametric-based  $K_i$  values. Two sets of parametric  $K_i$  values were accordingly generated and we presented a comparison between NLR-based and parametric-based  $K_i$  values for  $^{68}\text{Ga}$ -DOTATOC and  $^{68}\text{Ga}$ -DOTATATE. In a subset of 10 patients with 16 tumors, high correlation and agreement was found between the VOI and parametric-based  $K_i$  values (Fig. 1) and no significant bias was found for the two methods, neither for  $^{68}\text{Ga}$ -DOTATOC nor for  $^{68}\text{Ga}$ -DOTATATE. Consequently BFM and Patlak methods for computation of parametric images performed equally well and produced similar  $K_i$ -values both for  $^{68}\text{Ga}$ -DOTATOC and  $^{68}\text{Ga}$ -DOTATATE. The agreement and correlation between the two parametric methods (BFM and Patlak) was also tested and both methods were found to generate similar  $K_i$ -values. However, parametric images appeared to show a considerable overestimation for low  $K_i$  values and a slight underestimation for high  $K_i$  values compared to NLR (as seen in Supplemental Figs 1 and 2). A possible explanation for this is that for low tumor uptake, the time-activity curves obtained from

the 50% VOI in the dynamic images are a combination of the actual tumor uptake and spill-in from surrounding tissue. Since  $K_i$  in the surrounding liver tissue is much lower than in tumor tissue, VOI based analysis using NLR will probably underestimate tumor  $K_i$  values. Since the liver background in the parametric images is much lower the  $K_i$  values derived from the parametric images will to a much larger extent represent the actual tumor  $K_i$  and thus will be higher than the NLR values. In addition, VOIs were drawn independently in parametric and whole-body images. However, using the same VOIs in the dynamic and parametric images did not alter the conclusion, i.e., parametric  $K_i$  values remained higher than NLR-based  $K_i$  values.

Many NET patients develop liver metastases but, because of the moderately high physiological liver uptake of  $^{68}\text{Ga}$ -DOTATOC/DOTATATE, the detection of liver lesions may be jeopardized, especially when they are small. Also, this makes it challenging to evaluate therapy response because the physiological liver background will affect the accuracy of the tumor uptake measurements. The tumor-to-liver ratio for whole-body SUV and parametric  $K_i$  images were therefore compared and the latter were found to provide considerably better image contrast for both tracers (Figs. 3 and 4), although this was most apparent for  $^{68}\text{Ga}$ -DOTATATE. As previously shown (6) the uptake of  $^{68}\text{Ga}$ -DOTATOC /DOTATATE in both liver and tumors is more or less constant from 40 min p.i., with a possible small continuing increase for tumors. Therefore, using other uptake times for the SUV image in this comparison would not have affected contrast, but noise would increase for later time points. Consequently, the parametric  $K_i$  images can additionally be used to better visualize liver metastases. However, for its clinical implementation, automated methods for image-derived input function definition, such as previously presented for example for  $^{15}\text{O}$ -water myocardial blood flow imaging (44), need to be developed.

Because of the dynamic acquisition protocol required to generate the parametric  $K_i$  images, the whole abdomen or thorax may not be included for examination. The anatomical region that may be included for examination is therefore limited to the 15.5 cm axial field of view of the current PET/CT system, which reduces the clinical usefulness of the method. However, the recent generation of PET/CT and PET/MRI scanners, providing up to 25 cm axial field of view, is a considerable improvement in this respect. Also, an alternative acquisition protocol may be applied to generate whole-body parametric Patlak  $K_i$  images, based on a short dynamic scan over the thorax followed by fast serial whole-body scanning. This will be the subject of future work.

## **CONCLUSION**

Quantitatively accurate parametric  $K_i$  images, showing  $K_i$  of  $^{68}\text{Ga}$ -DOTATOC or  $^{68}\text{Ga}$ -DOTATATE at the voxel level, can be computed using the methods presented in the present work. In addition, the parametric methods reduced the signal from the liver for both tracers, providing better tumor-to-liver contrast in the parametric  $K_i$  images than in whole-body images. Further methodological developments are necessary for clinical implementation of parametric  $K_i$  images to be feasible.

## **DISCLOSURE**

No financial disclosures.

## **ACKNOWLEDGEMENT**

The authors would like to express their gratitude to Mimmi Lindholm, Annie Bjurebäck, Maj Wiberg, Lars Lindsjö and Marie Åhlman for their assistance in the PET/CT examinations.



## REFERENCES

1. Sundin A, Rockall A. Therapeutic monitoring of gastroenteropancreatic neuroendocrine tumors: the challenges ahead. *Neuroendocrinology*. 2012;96:261-271.
2. Yao JC, Hassan M, Phan A, et al. One hundred years after "carcinoid": epidemiology of and prognostic factors for neuroendocrine tumors in 35,825 cases in the United States. *J Clin Oncol*. 2008;26:3063-3072.
3. Bodei L, Pepe G, Paganelli G. Peptide receptor radionuclide therapy (PRRT) of neuroendocrine tumors with somatostatin analogues. *Eur Rev Med Pharmacol Sci*. 2010;14:347-351.
4. Bodei L, Mueller-Brand J, Baum RP, et al. The joint IAEA, EANM, and SNMMI practical guidance on peptide receptor radionuclide therapy (PRRNT) in neuroendocrine tumours. *Eur J Nucl Med Mol Imaging*. 2013;40:800-816.
5. van Essen M, Sundin A, Krenning EP, Kwekkeboom DJ. Neuroendocrine tumours: the role of imaging for diagnosis and therapy. *Nat Rev Endocrinol*. 2014;10:102-114.
6. Velikyan I, Sundin A, Sorensen J, et al. Quantitative and qualitative inpatient comparison of <sup>68</sup>Ga-DOTATOC and <sup>68</sup>Ga-DOTATATE: net uptake rate for accurate quantification. *J Nucl Med*. 2014;55:204-210.

7. Al-Nahhas A. Nuclear medicine imaging of neuroendocrine tumours. *Clin Med (Lond)*. 2012;12:377-380.
8. Oberg K. Gallium-68 somatostatin receptor PET/CT: is it time to replace (111)Indium DTPA octreotide for patients with neuroendocrine tumors? *Endocrine*. 2012;42:3-4.
9. Schreiter NF, Brenner W, Nogami M, et al. Cost comparison of 111In-DTPA-octreotide scintigraphy and 68Ga-DOTATOC PET/CT for staging enteropancreatic neuroendocrine tumours. *Eur J Nucl Med Mol Imaging*. 2012;39:72-82.
10. Gabriel M, Decristoforo C, Kendler D, et al. 68Ga-DOTA-Tyr3-octreotide PET in neuroendocrine tumors: comparison with somatostatin receptor scintigraphy and CT. *J Nucl Med*. 2007;48:508-518.
11. Ambrosini V, Campana D, Bodei L, et al. 68Ga-DOTANOC PET/CT clinical impact in patients with neuroendocrine tumors. *J Nucl Med*. 2010;51:669-673.
12. Kam BL, Teunissen JJ, Krenning EP, et al. Lutetium-labelled peptides for therapy of neuroendocrine tumours. *Eur J Nucl Med Mol Imaging*. 2012;39(suppl 1):S103-112.
13. Kwekkeboom DJ, Teunissen JJ, Bakker WH, et al. Radiolabeled somatostatin analog [177Lu-DOTA0,Tyr3]octreotate in patients with endocrine gastroenteropancreatic tumors. *J Clin Oncol*. 2005;23:2754-2762.

14. Kwekkeboom DJ, de Herder WW, Kam BL, et al. Treatment with the radiolabeled somatostatin analog [177 Lu-DOTA 0,Tyr3]octreotate: toxicity, efficacy, and survival. *J Clin Oncol.* 2008;26:2124-2130.
15. Bergsma H, van Vliet EI, Teunissen JJ, et al. Peptide receptor radionuclide therapy (PRRT) for GEP-NETs. *Best Pract Res Clin Gastroenterol.* 2012;26:867-881.
16. Kwekkeboom DJ, Bakker WH, Kam BL, et al. Treatment of patients with gastro-entero-pancreatic (GEP) tumours with the novel radiolabelled somatostatin analogue [177Lu-DOTA(0),Tyr3]octreotate. *Eur J Nucl Med Mol Imaging.* 2003;30:417-422.
17. Forrer F, Uusijarvi H, Storch D, Maecke HR, Mueller-Brand J. Treatment with 177Lu-DOTATOC of patients with relapse of neuroendocrine tumors after treatment with 90Y-DOTATOC. *J Nucl Med.* 2005;46:1310-1316.
18. Kwekkeboom DJ, Mueller-Brand J, Paganelli G, et al. Overview of results of peptide receptor radionuclide therapy with 3 radiolabeled somatostatin analogs. *J Nucl Med.* 2005;46 Suppl 1:62S-66S.
19. Bodei L, Cremonesi M, Grana CM, et al. Peptide receptor radionuclide therapy with (1)(7)(7)Lu-DOTATATE: the IEO phase I-II study. *Eur J Nucl Med Mol Imaging.* 2011;38:2125-2135.

20. Gabriel M, Andergassen U, Putzer D, et al. Individualized peptide-related-radionuclide-therapy concept using different radiolabelled somatostatin analogs in advanced cancer patients. *Q J Nucl Med Mol Imaging*. 2010;54:92-99.
21. Garske U, Sandstrom M, Johansson S, et al. Lessons on tumour response: imaging during therapy with (177)Lu-DOTA-octreotate. A case report on a patient with a large volume of poorly differentiated neuroendocrine carcinoma. *Theranostics*. 2012;2:459-471.
22. Chalkia MT, Stefanoyiannis AP, Chatziioannou SN, Round WH, Efstathopoulos EP, Nikiforidis GC. Patient-specific dosimetry in peptide receptor radionuclide therapy: a clinical review. *Australas Phys Eng Sci Med*. 2015;38:7-22.
23. Eisenhauer EA, Therasse P, Bogaerts J, et al. New response evaluation criteria in solid tumours: revised RECIST guideline (version 1.1). *Eur J Cancer*. 2009;45:228-247.
24. Gabriel M, Oberauer A, Dobrozemsky G, et al. 68Ga-DOTA-Tyr3-octreotide PET for assessing response to somatostatin-receptor-mediated radionuclide therapy. *J Nucl Med*. 2009;50:1427-1434.
25. Oberg K, Jelic S, Group EGW. Neuroendocrine gastroenteropancreatic tumors: ESMO clinical recommendations for diagnosis, treatment and follow-up. *Ann Oncol*. 2008;19 Suppl 2:ii104-105.

26. Belhocine T, Foidart J, Rigo P, et al. Fluorodeoxyglucose positron emission tomography and somatostatin receptor scintigraphy for diagnosing and staging carcinoid tumours: correlations with the pathological indexes p53 and Ki-67. *Nucl Med Commun.* 2002;23:727-734.
27. Haug AR, Auernhammer CJ, Wangler B, et al. 68Ga-DOTATATE PET/CT for the early prediction of response to somatostatin receptor-mediated radionuclide therapy in patients with well-differentiated neuroendocrine tumors. *J Nucl Med.* 2010;51:1349-1356.
28. Sandstrom M, Velikyan I, Garske-Roman U, et al. Comparative biodistribution and radiation dosimetry of 68Ga-DOTATOC and 68Ga-DOTATATE in patients with neuroendocrine tumors. *J Nucl Med.* 2013;54:1755-1759.
29. Lubberink M, Direcks W, Emmering J, et al. Validity of simplified 3'-deoxy-3'-[18F]fluorothymidine uptake measures for monitoring response to chemotherapy in locally advanced breast cancer. *Mol Imaging Biol.* 2012;14:777-782.
30. Gunn RN, Sargent PA, Bench CJ, et al. Tracer kinetic modeling of the 5-HT1A receptor ligand [carbonyl-11C]WAY-100635 for PET. *Neuroimage.* 1998;8:426-440.
31. Boellaard R, Oyen WJ, Hoekstra CJ, et al. The Netherlands protocol for standardisation and quantification of FDG whole body PET studies in multi-centre trials. *Eur J Nucl Med Mol Imaging.* 2008;35:2320-2333.

- 32.** Gunn RN, Gunn SR, Cunningham VJ. Positron emission tomography compartmental models. *J Cereb Blood Flow Metab.* 2001;21:635-652.
- 33.** Heidari P, Wehrenberg-Klee E, Habibollahi P, Yokell D, Kulke M, Mahmood U. Free somatostatin receptor fraction predicts the antiproliferative effect of octreotide in a neuroendocrine tumor model: implications for dose optimization. *Cancer Res.* 2013;73:6865-6873.
- 34.** Henze M, Dimitrakopoulou-Strauss A, Milker-Zabel S, et al. Characterization of <sup>68</sup>Ga-DOTA-D-Phe1-Tyr3-octreotide kinetics in patients with meningiomas. *J Nucl Med.* 2005;46:763-769.
- 35.** Koukouraki S, Strauss LG, Georgoulas V, Eisenhut M, Haberkorn U, Dimitrakopoulou-Strauss A. Comparison of the pharmacokinetics of <sup>68</sup>Ga-DOTATOC and [<sup>18</sup>F]FDG in patients with metastatic neuroendocrine tumours scheduled for <sup>90</sup>Y-DOTATOC therapy. *Eur J Nucl Med Mol Imaging.* 2006;33:1115-1122.
- 36.** Koukouraki S, Strauss LG, Georgoulas V, et al. Evaluation of the pharmacokinetics of <sup>68</sup>Ga-DOTATOC in patients with metastatic neuroendocrine tumours scheduled for <sup>90</sup>Y-DOTATOC therapy. *Eur J Nucl Med Mol Imaging.* 2006;33:460-466.
- 37.** Patlak CS, Blasberg RG, Fenstermacher JD. Graphical evaluation of blood-to-brain transfer constants from multiple-time uptake data. *J Cereb Blood Flow Metab.* 1983;3:1-7.

- 38.** Gunn RN, Lammertsma AA, Hume SP, Cunningham VJ. Parametric imaging of ligand-receptor binding in PET using a simplified reference region model. *Neuroimage*. 1997;6:279-287.
- 39.** Watabe H, Jino H, Kawachi N, et al. Parametric imaging of myocardial blood flow with <sup>15</sup>O-water and PET using the basis function method. *J Nucl Med*. 2005;46:1219-1224.
- 40.** Patlak CS, Blasberg RG. Graphical evaluation of blood-to-brain transfer constants from multiple-time uptake data. Generalizations. *J Cereb Blood Flow Metab*. 1985;5:584-590.
- 41.** Kratochwil C, Stefanova M, Mavriopoulou E, et al. SUV of [68Ga]DOTATOC-PET/CT Predicts Response Probability of PRRT in Neuroendocrine Tumors. *Mol Imaging Biol*. 2015;17:313-318.
- 42.** Oksuz MO, Winter L, Pfannenbergl C, et al. Peptide receptor radionuclide therapy of neuroendocrine tumors with (90)Y-DOTATOC: is treatment response predictable by pre-therapeutic uptake of (68)Ga-DOTATOC? *Diagn Interv Imaging*. 2014;95:289-300.
- 43.** Velikyan I, Sundin A, Eriksson B, et al. In vivo binding of [68Ga]-DOTATOC to somatostatin receptors in neuroendocrine tumours--impact of peptide mass. *Nucl Med Biol*. 2010;37:265-275.

- 44.** Harms HJ, Knaapen P, de Haan S, Halbmeijer R, Lammertsma AA, Lubberink M. Automatic generation of absolute myocardial blood flow images using [15O]H<sub>2</sub>O and a clinical PET/CT scanner. *Eur J Nucl Med Mol Imaging*. 2011;38:930-939.



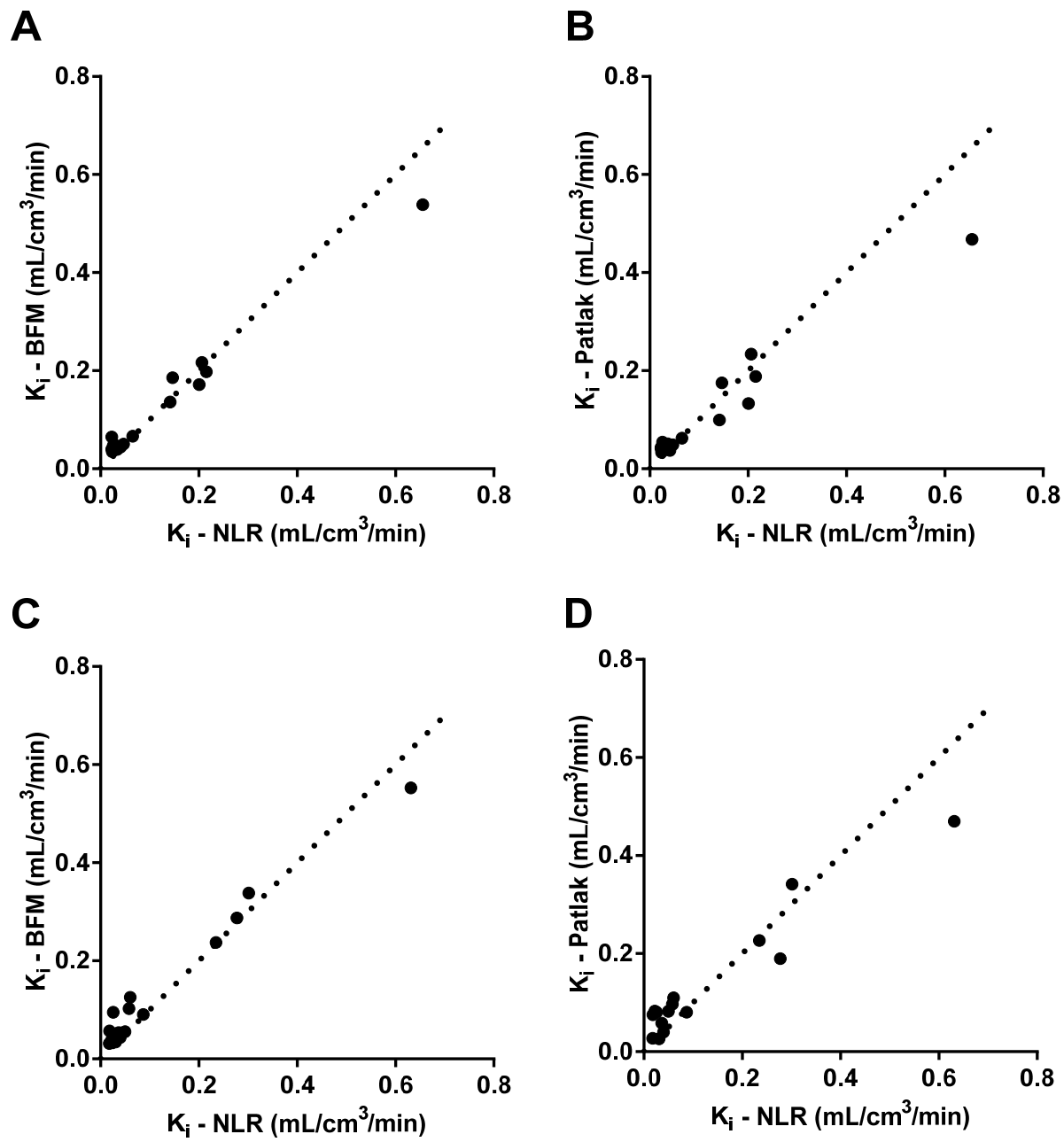


Figure 1: Correlation between NLR and parametric based (BFM and Patlak)  $K_i$  values for <sup>68</sup>Ga-DOTATOC (A-B) and <sup>68</sup>Ga-DOTATATE (C-D). The dashed lines represent lines of identity.

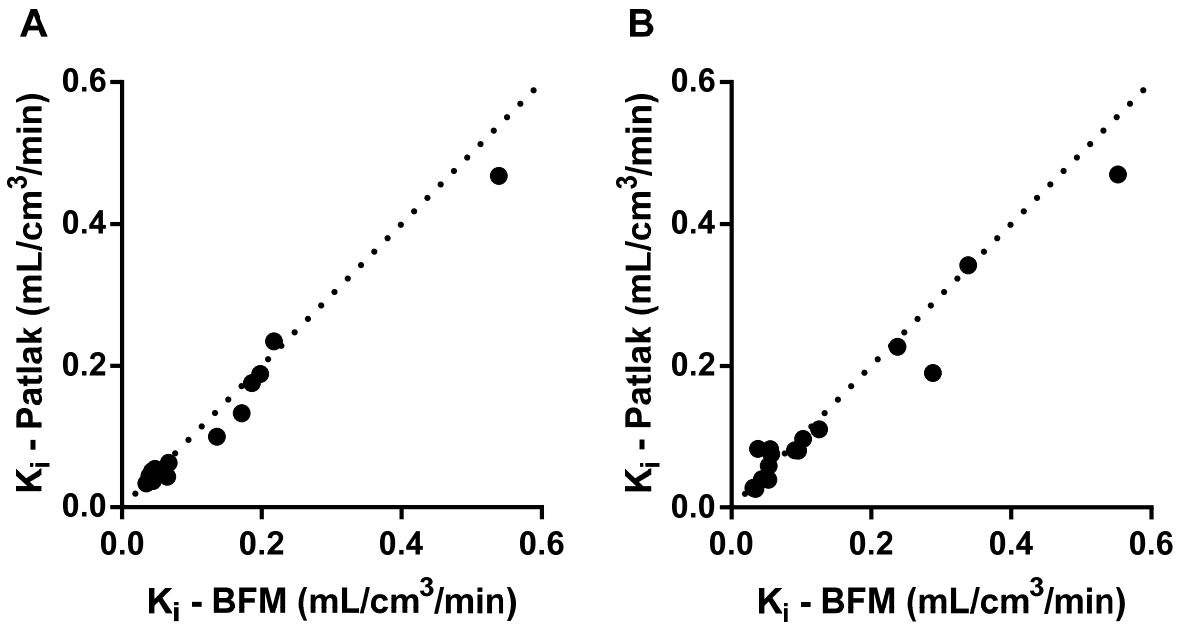


Figure 2: Correlation between parametric net influx rate,  $K_i$ , in tumor VOIs determined by basis function method (BFM) and Patlak analysis for <sup>68</sup>Ga-DOTATOC (A) and <sup>68</sup>Ga-DOTATATE (B). The dashed lines represent line of identity.

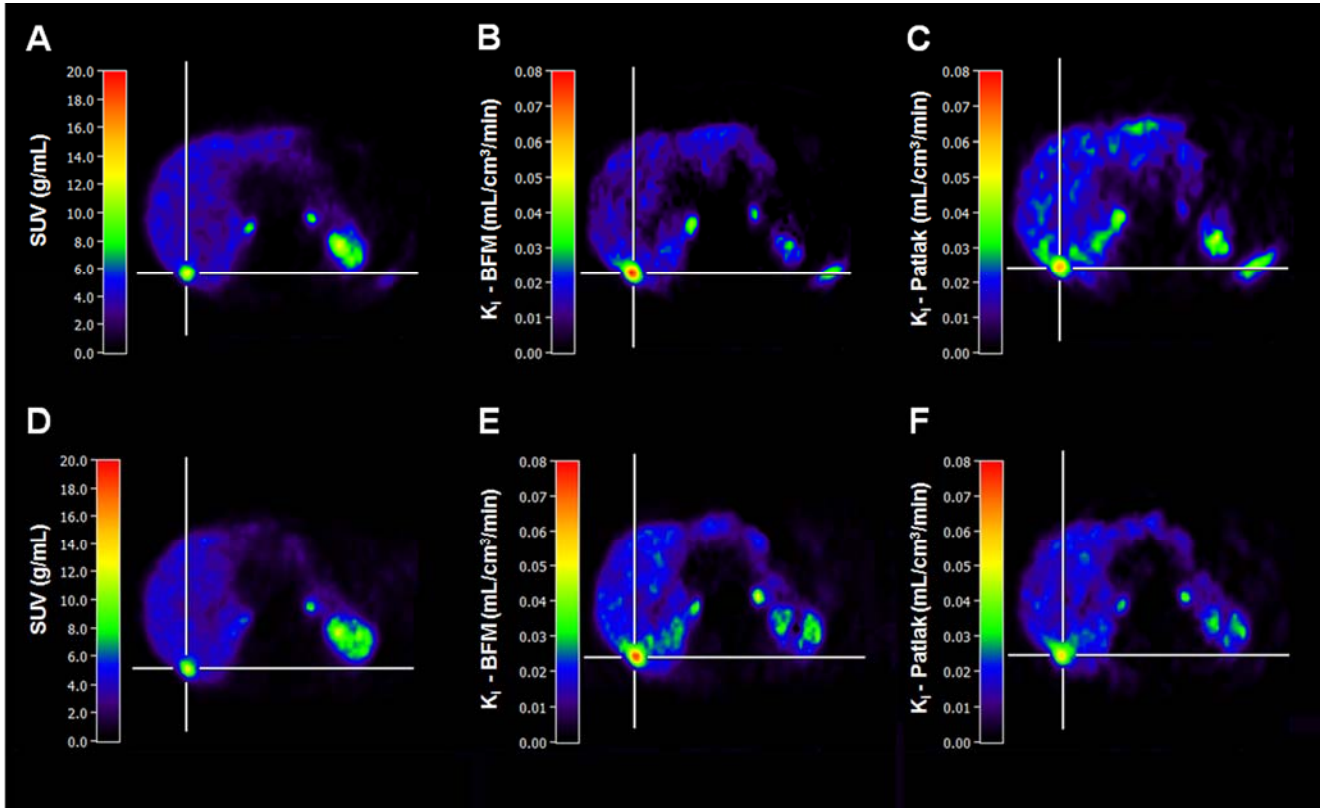


Figure 3: Representative transaxial images of the liver obtained from a static whole-body examination at 1 h post injection (A:  $^{68}\text{Ga}$ -DOTATOC; D:  $^{68}\text{Ga}$ -DOTATATE) and parametric  $K_1$  images based on basis function method (B:  $^{68}\text{Ga}$ -DOTATOC; E:  $^{68}\text{Ga}$ -DOTATATE) and Patlak method (C:  $^{68}\text{Ga}$ -DOTATOC; F:  $^{68}\text{Ga}$ -DOTATATE), showing comparison of image contrast.

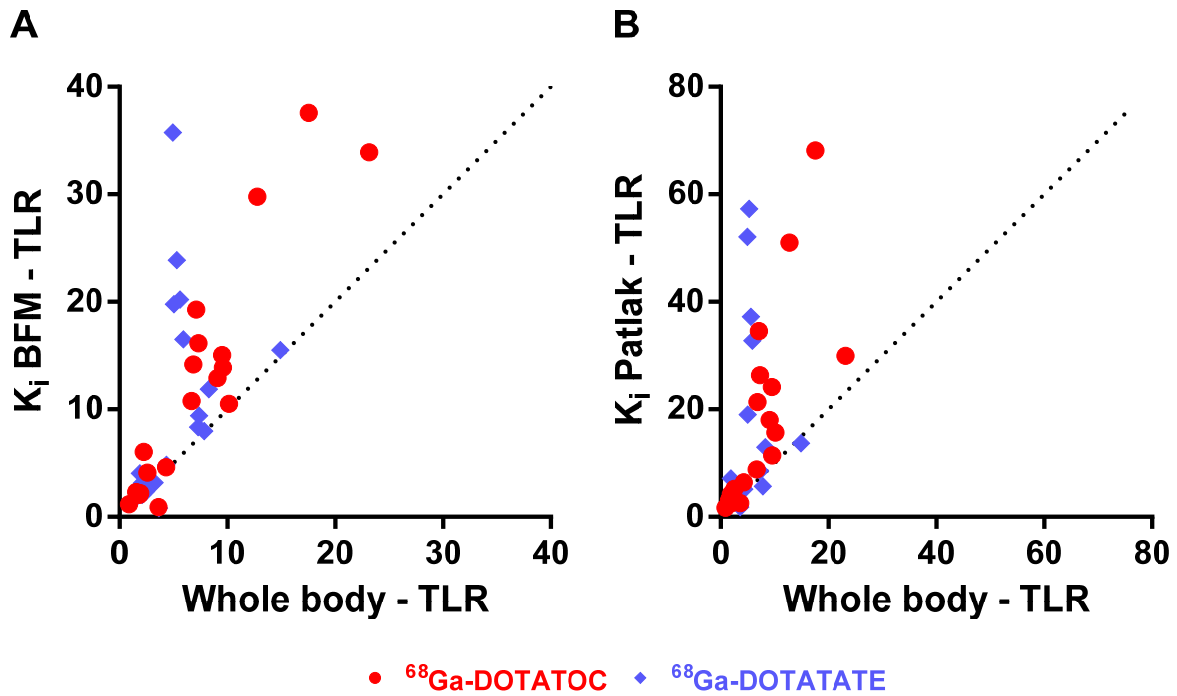
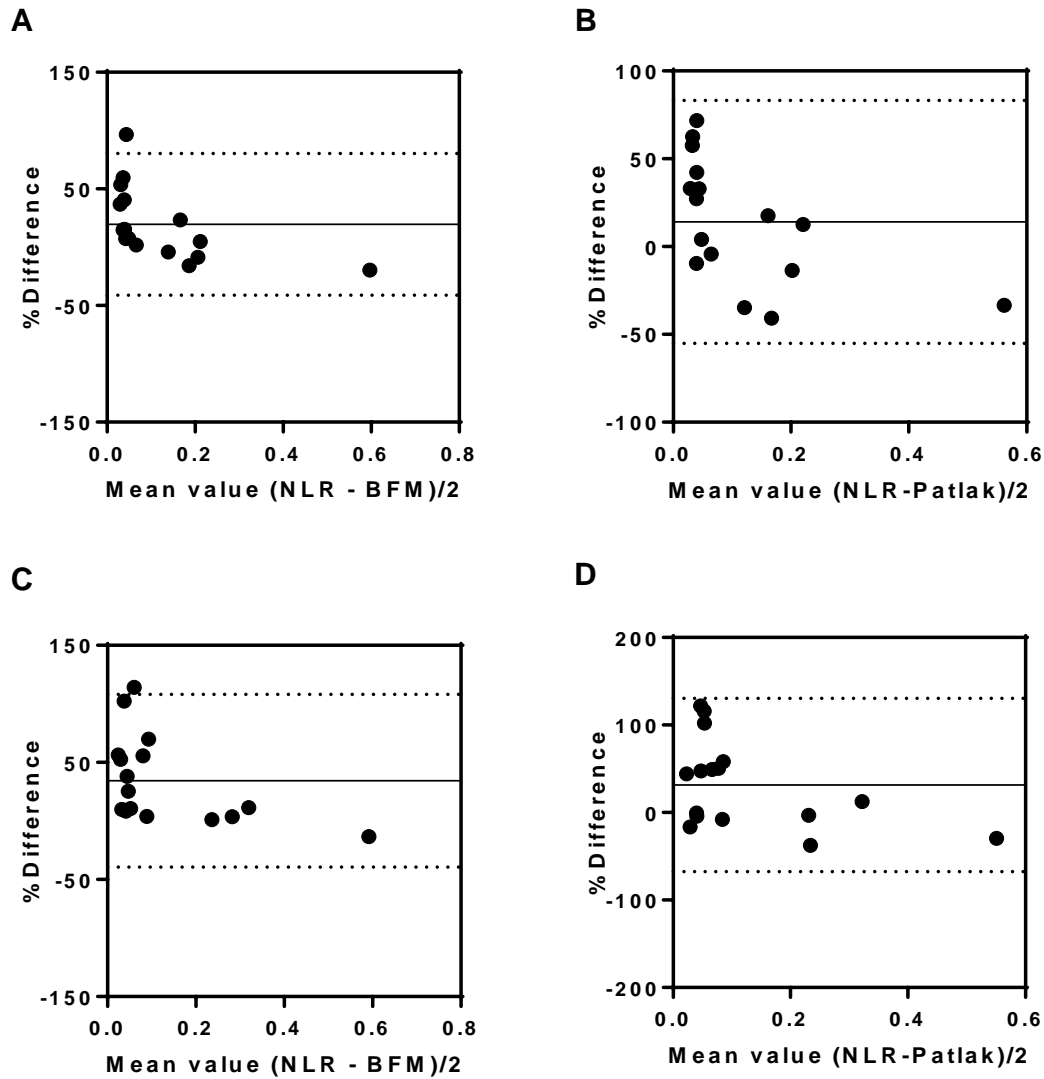


Figure 4: Tumor-to-liver ratio (TLR) for whole body and parametric  $K_i$  images for BFM (A) and Patlak (B) both for  $^{68}\text{Ga}$ -DOTATOC (A, B) and  $^{68}\text{Ga}$ -DOTATATE (A, B). The dashed lines represent lines of identity. Mean tumor to liver contrasts were 1.6 (A, red dot), 2.0 (A, blue diamond), 2.3 (B, red dot), and 3.0 (B, blue diamond) times higher in the parametric  $K_i$  images than in the whole-body images.

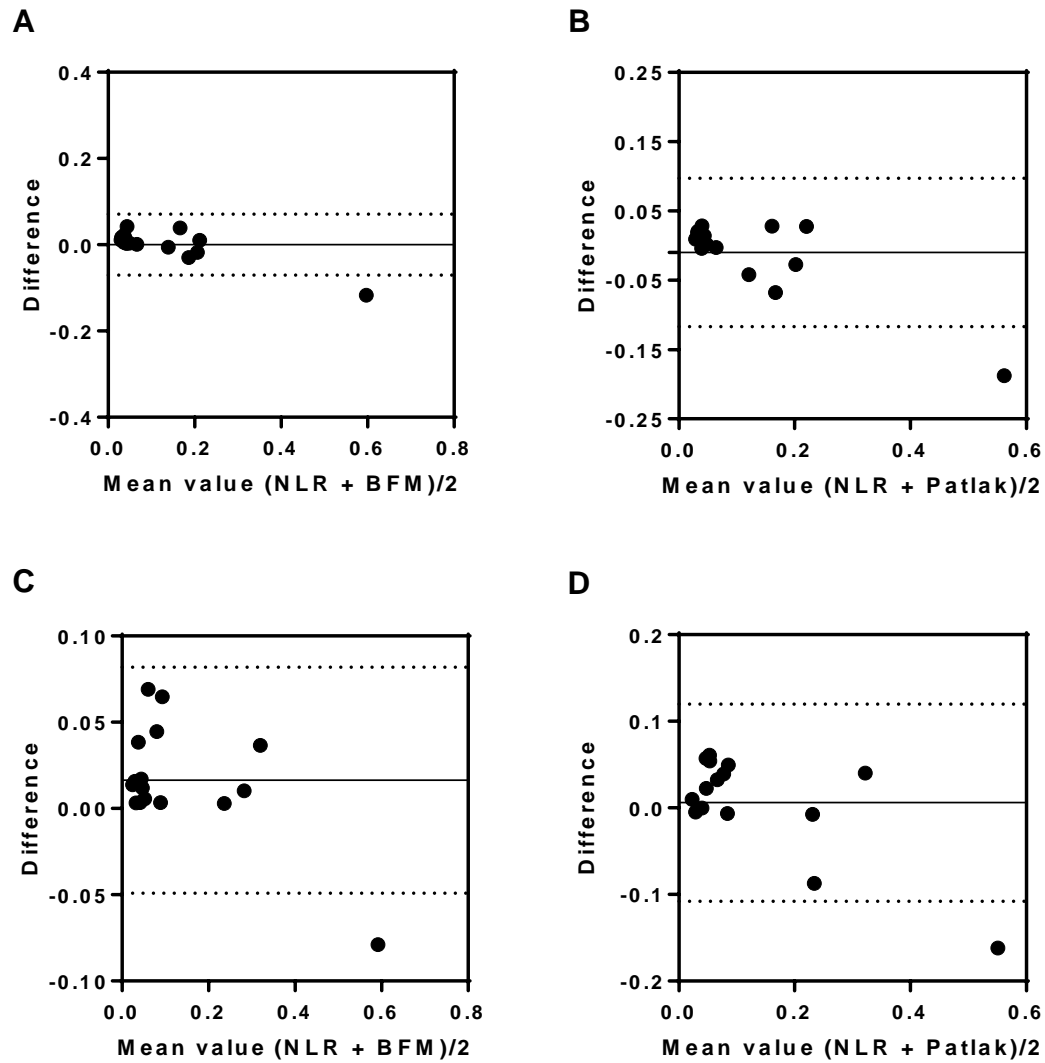
Table 1: Pearson correlation coefficients ( $R^2$ ), Deming regression slope and bias between the tumor VOI (NLR) and parametric based (BFM and Patlak)  $K_i$ -values.

		<b>Correlation (<math>R^2</math>)</b>	<b>Slope (95% CI<sup>1</sup>)</b>	<b>Bias (95% CI<sup>1</sup>)</b>
<b><sup>68</sup>Ga-DOTATOC</b>	BFM	0.98	0.81 (0.75 to 0.87)	0.00 (-0.07 to 0.07)
	Patlak	0.95	0.71 (0.62 to 0.80)	0.00 (-0.12 to 0.10)
<b><sup>68</sup>Ga-DOTATATE</b>	BFM	0.97	0.88 (0.79 to 0.96)	0.02 (-0.05 to 0.08)
	Patlak	0.92	0.74 (0.62 to 0.86)	0.00 (-0.11 to 0.12)

<sup>1</sup> Confidence interval



Supplemental Figure 1: Bland-Altman plot of percentage difference in  $K_i$ -values derived using non-linear regression (NLR) and parametric methods (BFM and Patlak) for  $^{68}\text{Ga}$ -DOTATOC (A-B) and  $^{68}\text{Ga}$ -DOTATATE (C-D). Solid lines represents mean difference and the dashed lines represent  $\pm 2$  SD-values.



Supplemental Figure 2: Bland-Altman plot of difference in  $K_i$ -values derived using non-linear regression (NLR) and parametric methods (BFM and Patlak) for  $^{68}\text{Ga}$ -DOTATOC (A-B) and  $^{68}\text{Ga}$ -DOTATATE (C-D). Solid lines represents mean difference and the dashed lines represent  $\pm 2$  SD-values.